MIT Libraries | DSpace@MIT

MIT Open Access Articles

Non-linear collisionless plasma wakes of small particles

Massachusetts Institute of Technology

Non-linear collisionless plasma wakes of small particles

I H Hutchinson

Plasma Science and Fusion Center and
Department of Nuclear Science and Engineering,
Massachusetts Institute of Technology, Cambridge, MA, USA

Abstract

The wake behind a spherical particle smaller than the Debye length (λ_{De}) in flowing plasma is calculated using a particle-in-cell code. The results with different magnitudes of charge reveal substantial non-linear effects down to values that for a floating particle would correspond to a particle radius approximately $10^{-2}\lambda_{De}$. The peak potential in the oscillatory wake structure is strongly suppressed by non-linearity, never exceeding approximately 0.4 times the unperturbed ion energy. By contrast, the density peak arising from ion focusing can be many times the ambient. Strong heating of the ions occurs in the non-linear regime. Direct ion absorption by the particle is not important for the far wake unless the radius exceeds $10^{-1}\lambda_{De}$, and is therefore never significant (for the far wake) in the linear regime. Reasonable agreement with full-scale linear-response calculations are obtained in the linear regime. The wake wavelength is confirmed and an explanation, in terms of the conical potential structure, is proposed for experimentally-observed oblique alignment of different-sized grains.

1   Introduction and Background

The perturbation of a plasma by a moving charge, or equivalently the perturbation of a plasma flowing past a stationary charge, is a foundational plasma physics problem. For elementary point charges (electrons or ions), in a weakly coupled plasma, the response of the plasma, and the resulting drag on the charge, is accurately calculated using linear response theory. The Vlasov equations for the electrons and ions are solved in the standard linearized approximation to give a (Fourier transformed) linear dielectric constant $\epsilon(\mathbf{k}, \omega) = 1 + \chi_e + \chi_i$ (with χ the susceptibility), and the potential at a position $\mathbf{x}$ relative to a charge Q moving at velocity $\mathbf{v}_d$ relative to the plasma can be written[1]

$$\phi(\mathbf{x}) = \int \frac{\exp(i\mathbf{k}.\mathbf{x})Q}{(2\pi)^3 \epsilon_0 k^2 \epsilon(\mathbf{k}, \mathbf{k}.\mathbf{v}_d)} d^3k. \tag{1}$$

If instead of an elementary charge we consider a charged object, then under some circumstances it is reasonable to assume that this approach will still give a good approximation. In particular, if the radius of the object r_p is much smaller than the Debye length

$\lambda_{De} \equiv \sqrt{\epsilon_0 T_e/n_e e^2}$ then it may be possible to ignore its finite size, and the consequent absorption of plasma that will occur on its surface. If so, then whether or not the linear response formalism still applies depends just upon the magnitude of the object's charge. Dust particles in plasmas often satisfy $r_p \ll \lambda_{De}$, but they usually acquire a large charge sufficient to make the potential at their surface (when floating) typically a few times $-T_e/e$. It is then clear that near the object surface, linearity practically always fails.

The purpose of the present work is (1) to answer the further question, under what conditions does this non-linearity substantively change the *distant* response of the plasma potential, notably in the plasma wake? and (2) to solve the resulting non-linear wake structure. This enterprise is of considerable importance for understanding dust interactions in plasmas, since it is known that particles suspended in a plasma sheath, and hence in a region where ions are flowing with approximately the sound speed, attract other dust particles which lie in their wake[2, 3]. This phenomenon is attributed to a potential maximum arising in the wake.

Linear response formalism has long been used to solve for the far wake structure. [We shall not here address the important question of the change in the ion shielding of the particle as the ion drift increases from zero. That has been the subject of many studies.] Sanmartin and Lam (1971)[4] considered the situation of cold ion flow, and predicted a steep wave front at the ion-acoustic Mach angle for supersonic flow and two sets of waves. In sub-acoustic flow, waves were also predicted. Warm ions gave rise to wave damping. Chen, Langdon, and Lieberman (1973)[5] likewise performed analytic studies using linearized formalism, and for convenience a warm ion distribution that was uniform (a rectangle distribution) in velocity space. They too found two types of waves of different wavelength and predicted 'Cerenkov' (i.e. Mach) cones. Despite the linear approximations, the equations of these authors do not provide convenient quantitative analytic expressions for the wake form. Ishihara and Vladimirov (1997)[6] revived interest in this approach in the dusty plasma context as an explanation for the observed attraction of a downstream grain into the wake of another. Their analysis led to expressions representing oscillatory wakes with wavelength in the flow direction equal to

$$2\pi\lambda_{De}\sqrt{M^2 - 1}, \tag{2}$$

where $M \equiv v_d/\sqrt{T_e/m_i}$ is the drift Mach number (for supersonic flow). Their wakes have trailing crossed-wavelength oscillatory structures behind a Mach-cone. Xie et al (1999)[7] revisited this analysis and concluded that the wavelength in subsonic flow is simply

$$2\pi\lambda_{De}M \tag{3}$$

right up to $M = 1$. Lemons et al (2000)[8] obtained oscillatory wakes with longitudinal wavelength simply $2\pi\lambda_{De}M$ (eq 3) for supersonic flow, but with a combination of long and short wavelengths in two-dimensional cartesian subsonic flow (i.e. flow past charge-rods). For cylindrically symmetric two-dimensional flow (i.e. past spherical grains) they concluded that only the simple (3) wavelength contributes, whether subsonic or supersonic, and they obtained analytic approximations to the potential. Lapenta (2000)[9] used fluid approximations

solved in space (not k-space) and found the simple oscillation wavelength (3) and plotted specific amplitudes. Hou et al (2001)[10] used ion-fluid approximations in k-space and obtained similar results. They also considered grains possessing an electric dipole moment. In contrast to these approximations, Lampe et al (2000)[11] directly performed numerical integrations of eq (1) for a drifting Maxwellian, and plotted the results for different ion/electron temperature ratios (and collisionalities but here we are focussing on collisionless cases). They found oscillations with the simple wavelength (3) for both subsonic and supersonic flow, within a cone-shaped wake structure.

Even assuming a correct linear analysis, the question remains whether it really applies to practical cases, whether *non-linear* effects are significant, and if they are, what happens to the wake? Given how uncertain even the linear analytic analysis has proven to be, heuristic arguments can't with confidence estimate the importance of non-linearities or, when they are important, their effects. Therefore self-consistent non-linear calculations are needed. Winske et al (2000)[12] performed cartesian particle-in-cell (PIC) non-linear ion calculations in one and two dimensions: planar charge-sheets and cylindrical charge-rods. The electrons were taken to have *linearized* Boltzmann response. In one dimension they found in agreement with linearized theory a wavelength $2\pi\lambda_{De}M/\sqrt{1-M^2}$ for subsonic flow. (Note that the $\sqrt{1-M^2}$ factor is in the denominator, unlike the expression 2.) Charge-rods, however, gave wakes with simple oscillatory wavelength (eq 3) $\sim 2\pi\lambda_{De}M$. The two-dimensional calculations had peak potential amplitudes approximately $(1-3)\times 10^{-2}T_e/e$, but different charge magnitudes were studied only for the unphysical one-dimensional case. Subsequent numerical studies for charge-rods have been pursued for example by Miloch et al (2008)[13]. These numerical investigations considered the qualitative features of the linearized analysis to be verified, but did not address systematically the quantitative non-linear effects. One should note also that a charge-rod does not represent the geometry of a sphere, which is what typical dust grains most closely approximate, and the linearized analysis shows qualitative differences between charge-rods and point-charges. Hutchinson (2005)[14] observed in two-dimensional PIC simulations of spherical grains that though the wavelength was approximately as in eq. (3), the non-linear wake was not at all consistent with the linearized analyses. The simulation's wake amplitude was far smaller and it damped out more quickly.

Oscillatory wakes occur only if the ion temperature T_i is much smaller than the electron temperature T_e. This can be interpreted as minimizing ion Landau damping, although it can also be considered a requirement that orbits remain coherent. The oscillatory wake studies cited explored ratios typically $25 \leq T_e/T_i \leq 100$. Analytic linearized treatments with $T_i = 0$ give rise to a singularity on the symmetry axis that is resolved only with finite ion temperature. Grain radius smaller than the anticipated oscillation wavelength ($r_p \lesssim M\lambda_{De}$) appears also necessary to observe oscillations. Both of these quantitative constraints apply to typical dusty plasma experiments.

Experimental investigation of the wake structure is extremely difficult, and few direct measurements have been made. The potential can best be deduced from the dynamics of a second particle moving in the wake. A weakness is that this requires one to assume that wake-induced changes in ion drag force can be ignored, which is not obvious. Takahashi et

al (1998) showed by optical manipulation that non-reciprocal effects on particles in the wake region aligned them with the upstream particle[15]. Melzer et al (1999) showed transitions (induced by neutral pressure changes) between attracting and repelling wakes[16], and estimated attracting force on a particle with charge $2000e$ of 1.6×10^{-15}N at 40μm horizontal and 750μm vertical separation. Steinberg et al[17] observed identical particles, suspended in a sheath, undergoing transitions between horizontal, vertical, and oblique alignment as the discharge power was varied, as did Samarian et al[18]. Low gas pressure and power favors vertical alignment. Alignment angles to the vertical less than 45° were not observed. The (linear response) theory of Lampe et al[19] for like particles in confining wells indicates that anharmonic (steep wall) well structure is required but can then explain oblique alignment. Recently Kroll et al[20] have observed return transitions to vertical alignment from metastable oblique alignment states that again have angles no less than 45° for like particles. Hebner and Riley (2003-4)[21, 22], in contrast, observed the dynamics of two interacting particles at low neutral pressure, moving in one horizontal dimension at almost fixed (but different) heights determined by the various *different* sizes of the particles. Like Melzer's, their observations were consistent with an interaction consisting of two parts (1) a repulsive Yukawa-potential force that operates reciprocally on both particles, and (2) a non-reciprocal attractive force on the downstream particle arising from the upstream particle's wake. They were able to deduce quantitatively these potentials (strictly speaking, the forces). The peak potential was fitted to be 21mV (in a $T_e = 3$eV plasma). They found that for large vertical separations the particles' horizontal equilibrium positions became offset from perfect vertical alignment by angles as small as $\sim 15^o$ which is not explicable by the analysis of ref [19].

The work reported here uses a PIC code in three dimensions to calculate the entire wake structure in a collisionless plasma behind spherical particles of a whole range of charges and sizes (smaller than λ_{De}). Subsonic and supersonic drift velocities are investigated. Strong saturation of the wake amplitude is observed for some experimentally-relevant parameters. A comparison with linear calculations is shown for small charge-magnitude. The domain of validity of the linearized approach is identified and the onset of non-linear effects is studied.

2   COPTIC Code

The program used to solve for the non-linear wakes in this work is a new Cartesian-mesh Oblique-boundary Particle and Thermals In Cell (COPTIC) code. This description refers to its three-dimensional cartesian grid on which the potential is represented, but that it can include objects of arbitrary shape whose boundaries can be oblique to the mesh directions. Many cartesian codes approximate such domain-boundaries rather crudely as staircases of connected cell-boundaries. COPTIC instead uses difference equations for the potential and electric field equivalent to the Shortley-Weller approximation that gives second-order accuracy[23] in solving the Poisson equation and interpolating the resulting field adjacent to oblique boundaries. It uses locally adjusted difference stencils accounting for the actual position, orientation, and boundary condition on both sides of a boundary that crosses the stencil. This allows reasonably accurate representation of oblique and curved surfaces such

as spheres, even when their size is not much smaller than the mesh spacing. Fig. 1 illustrates the challenging cases used here.
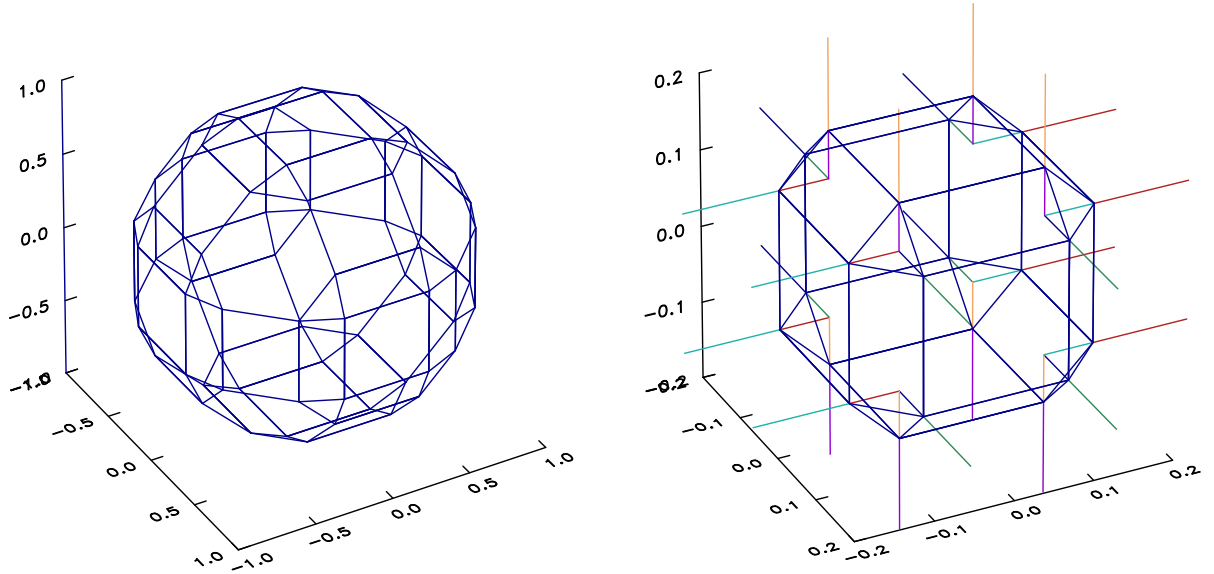

Figure 1: COPTIC representation of spheres of radius $r_p = 1$ and $r_p = 0.2$ on coarse meshes relative to their size. The wire frame joins vertices consisting of the intersections of the spheres with the mesh difference stencils. On the $r_p = 0.2$ figure the intercepted stencils themselves are also drawn.

COPTIC uses continuous analytic objects like spheres or cylinders to define geometric domains such as the the plasma region outside a particle. It thus knows exactly (to machine precision, yet with minimal computational effort) when an ion crosses an object boundary, for example when it hits a solid grain. The mesh can be specified as non-uniform (but still cartesian), to provide greater field-resolution in important areas such as near the particle surface. Resulting small self-forces in transitional areas do not prove to be significant.

In addition to finite-size objects, point charges can be incorporated. These are dealt with through the PPPM technique[24]. The field they give rise to is evaluated analytically for inclusion in the particle dynamics. Their potential is not represented by the Poisson solution on the mesh; the analytic potential is added to the potential grid after solution for purposes of display. In this way accurate dynamics are obtained without the mesh being required to resolve or represent the point-charge potential.

As in all PIC codes, the particle species, in this case ions of charge $q = Ze$, are advanced by the equation of motion

$$m\frac{d\mathbf{v}}{d\mathbf{x}} = q\mathbf{E} = -q\nabla\phi. \tag{4}$$

In the present work, no magnetic field is present. The potential is found as the solution of

$$\nabla^2\phi = -(qn_i - en_e)/\epsilon_0, \tag{5}$$

5

with the ion density, n_i, obtained from the particle representation by a Cloud-in-Cell assignment of charge to the mesh. The electrons are taken to be thermal so their density is given by a (non-linear) Boltzmann factor:

$$n_e = Z n_{i\infty} \exp(e\phi/T_e) \tag{6}$$

relative to the distant unperturbed ion density $n_{i\infty}$. Various types of boundary condition on ϕ are possible. In this work, the potential is fixed on the object representing the particle, and it has a particular component of its gradient set to zero at the outer boundary which is the mesh outer edge. This component is in the drift direction, $\hat{\mathbf{z}}$, at the ends (i.e. normal to boundaries which are perpendicular to the external drift velocity). At the sides (boundaries tangential to the drift) it is in the direction $M\hat{\mathbf{z}}+\hat{\mathbf{r}}$, where $\hat{\mathbf{r}}$ is the cylindrical radial direction. This oblique choice acts approximately as a non-reflecting boundary condition for the ion acoustic perturbations of the wake, to mock up an infinite plasma domain. On large enough meshes, the outer boundary condition is unimportant, as has been verified through different code runs. But the choice here is taking advantage both of the cylindrical symmetry of the problem (even though the mesh and domain lacks that rotational symmetry and it is not specifically imposed on the solution) and also of the observed form of the solution, to provide better accuracy on a domain of limited size. Most calculations are done with 32 million ions on a $44 \times 44 \times 96$ cell grid chosen to resolve the particle locally and the Debye length everywhere. This grid has total side length $10 \times 10 \times 25$ Debye lengths. See Fig. 2.

Particle advance and potential solution are carried out alternately in a standard leap-frog scheme[24]. Ions are injected from the outer boundary with spatial and velocity distribution that represents a uniform Maxwellian external plasma drifting in the $\hat{z}$-direction. Ions that leave the plasma domain in the present calculations are lost, being replaced by the constant injection rate. The code is advanced in time until a steady state is reached, after typically 2000 time-steps. That these states are observed to be steady, rather than unsteady flows, is a physically significant result. But the demonstration that unsteady fluctuations do not occur constitutes the only pay-off in return for the computational inefficiency of using a fully three-dimensional code on what is, short of spontaneous symmetry breaking, a two-dimensional problem (cylindrically symmetric about the flow direction). In short, COPTIC's three-dimensional capabilities are not really essential for this problem. We sometimes plot quantities averaged over some number of converged particle steps and averaged over the ignorable angle, to reduce their noise.

3 Non-linear Wake Results

Calculations are performed in normalized units for velocity $v \to v/\sqrt{T_e/m_i}$, and potential $\phi \to \phi/(T_e/e)$. Lengths can be considered normalized to some arbitrary scale length. The Debye length is set at 10 units of length. A spherical object of radius r_p and specified potential (uniform on its surface) ϕ_p relative to infinity, is placed with center at the origin within a cuboidal domain $-50 < x, y < 50$, $-50 < z < 200$. Figure 2 shows a rendering of the potential on a plane through the domain at $x \approx 0$. We see the strong negative potential
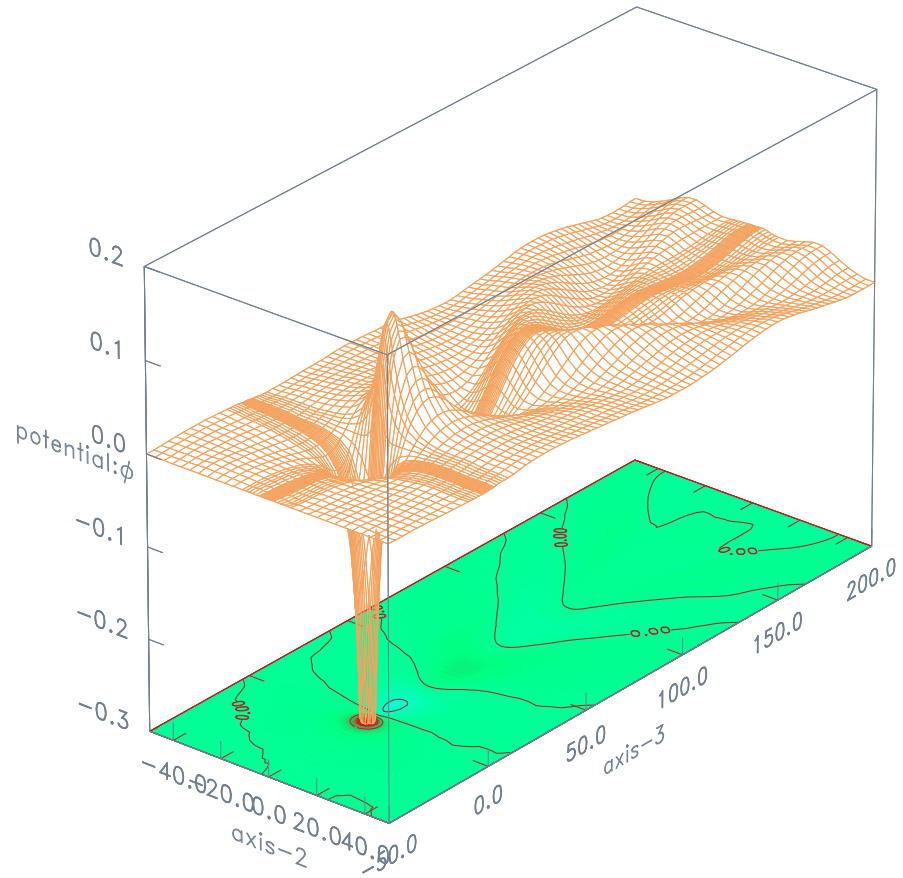
Figure 2: Potential on a fixed, $x = 0$, plane through the object. Parameters: $\lambda_{De} = 10$, $r_p = 1$, $\phi_p = -1$, $M = 1$, normalized units; $T_i/T_e = 0.01$.

of the sphere itself (truncated at the display box), and then immediately downstream a positive peak of the potential arising from ion focusing by the attractive (negative) potential perturbation of the sphere. Thereafter the wake has an oscillatory character with cone-shaped wave-fronts. The two-dimensional representation resembles a water wake.
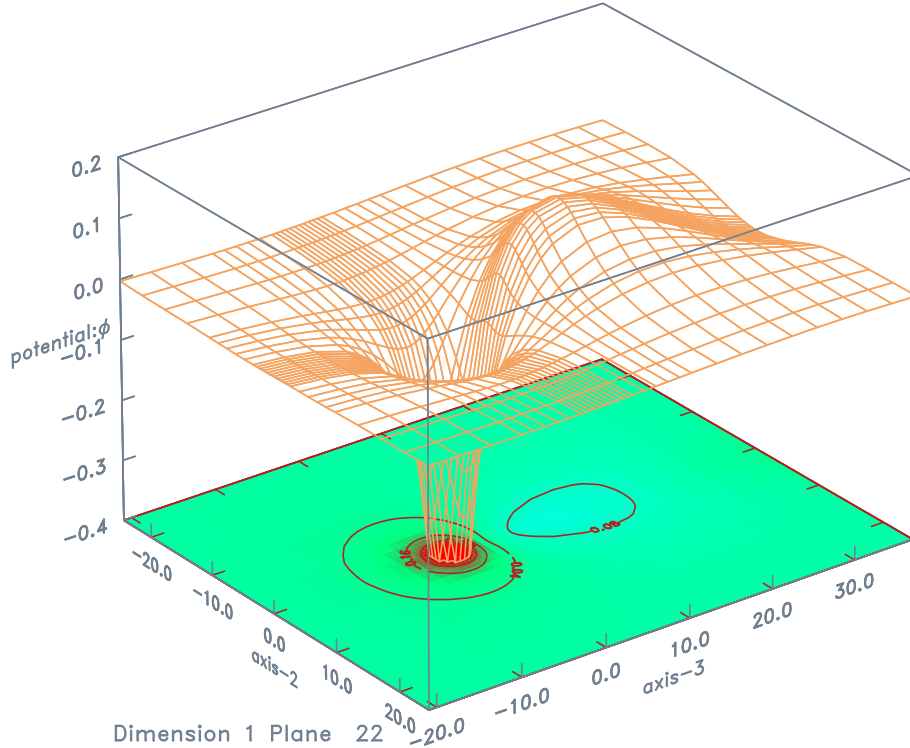

Figure 3: Close-up of potential on the plane $x = 0$, to show unequal mesh spacing. Parameters as in Fig. 2.

In Figure 3 we show an expanded view of the region of the object and potential peak. The individual lines of the web rendering are at the mesh positions, showing how the unequal mesh spacing is able to resolve the potential locally.

If the wake were linear, then its amplitude would be proportional to the sphere potential. To illustrate the non-linearity of the present model, in Figure 4 we plot the potential normalized to the potential on the sphere, which would be independent of ϕ_p in a linear system. (Here and in some other figures the label character λ is shorthand for the electron Debye length λ_{De}.) We see that even at the lowest potential, this system is not quite in a linear regime. Normalized potential is not quite independent of ϕ_p. The relative potential perturbation amplitude is slightly higher than the next-lowest potential result. At the lowest sphere potential, the potential perturbation at the peak is approximately $2 \times 10^{-2} T_e/e$. Unfortunately discreteness noise is already becoming significant at these lower potentials, for this systematic series of runs; so one cannot proceed to still lower perturbation levels without more expensive calculations using more particles to lower the noise. Such a run,
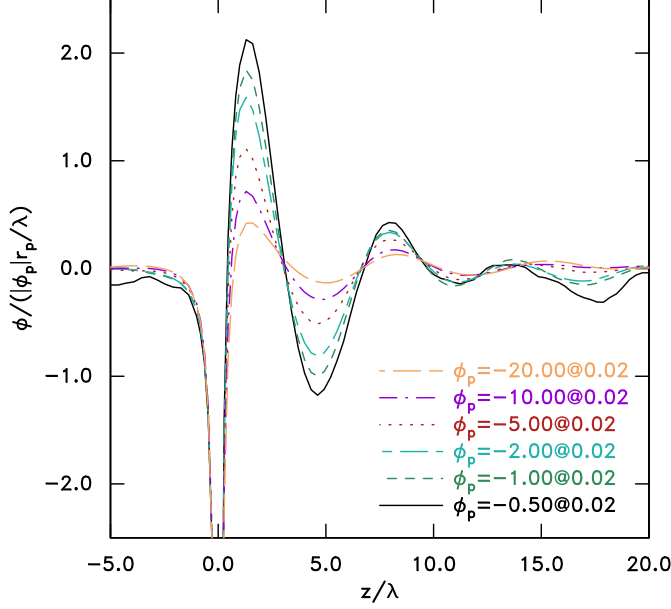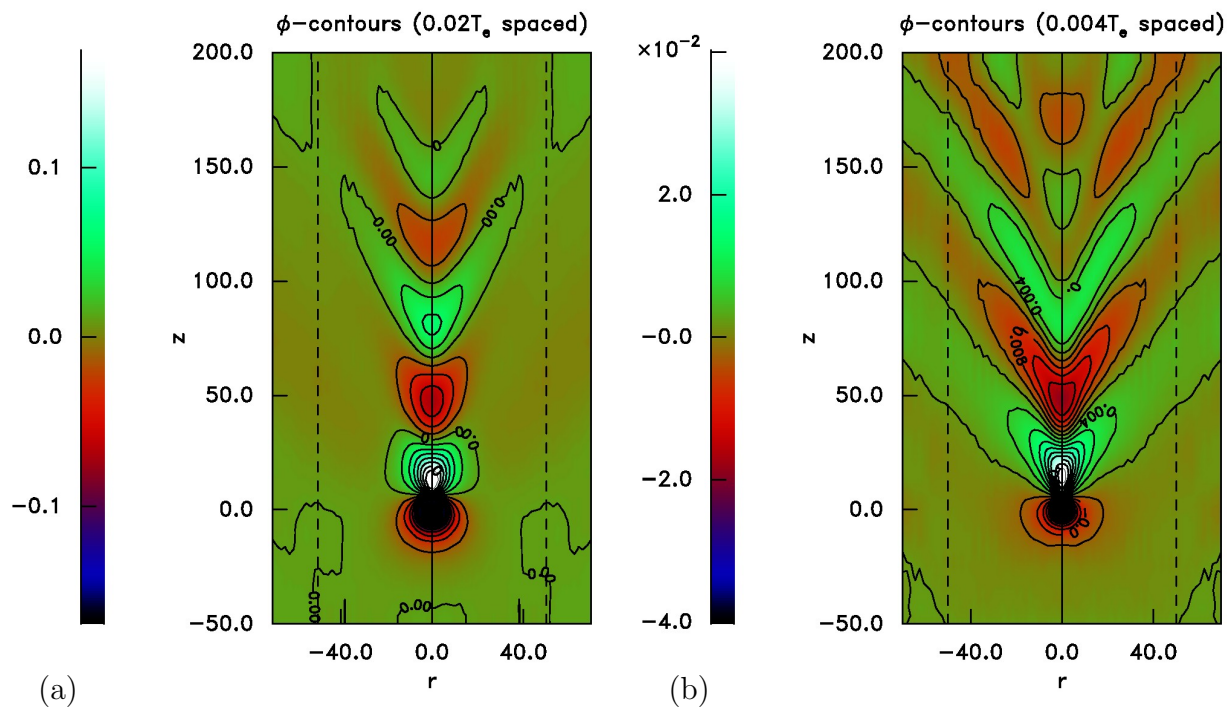
8

Figure 4: Normalized potential along the $x = y = 0$ axis, for different sphere potentials. Here $T_e/T_i = 100$, $M = 1$, $r_p = 0.02\lambda_{De}$.

at half the lowest particle charge gives a peak normalized potential the same as in figure 4 within uncertainty. So it is a good approximation to take the lowest ϕ_p case as linear. It should be noted that for low ϕ_p, noise causes a low level of effective collisionality which somewhat enhances the spatial damping of the distant wake.

Figure 5 shows contours of potential averaged in angle about the z-axis for two values of the potential on the sphere. [The plot includes a mirror image plotted at negative r purely for perceptual and aesthetic purposes. Radii with magnitude greater than 50 — outside the dashed lines — arise only from the corners of the rectangular grid. They, and the regions close to the top boundary, might be distorted by boundary proximity.] In 5(a) $\phi_p = -2$, and there are strong non-linear effects that limit the amplitude of the wake (as will be shown in a moment). Nevertheless, the wake's geometric form is only modestly different from 5(b) $\phi_p = -0.2$ which is a case in which the non-linear effects are weak. The non-linear case shows rather more rapid decay of the wake perturbation in the radial direction.

If finite size of the object were negligible, because $r_p \ll \lambda_{De}$, then the wake would depend only upon the object's charge, which could be expressed, accounting for the first order correction arising from Debye shielding, as $Q = 4\pi\epsilon_0 r_p \phi_p(1 + r_p/\lambda_{De})$. To establish the extent to which this approximation actually applies, equivalent calculations have been performed with either of two different finite-radius spheres, $r_p = 0.1\lambda_{De}$ and $r_p = 0.02\lambda_{De}$, or with a point charge, which we refer to as $r_p/\lambda_{De} = 0$. For each of these cases, the effective charge Q is varied by varying the potential at the object radius. Obviously, the main physical difference between these cases is that the finite objects absorb ions that collide with them. The point charge does not.

9

Figure 5: Contours of potential averaged in rotational angle for parameters $\lambda_{De} = 10$, $r_p = 1$, $M = 1$, $\phi_p = -2$(a), -0.2(b), normalized units; $T_i/T_e = 0.01$. The shape differences between a non-linearly saturated form (a) and a nearly linear form (b) are modest.

10

As a quantitative measure of the amplitude of the wake, we choose the immediate down-stream potential peak, which happens also always to be the maximum potential in the domain, ϕ_{max}. As Figure 4 indicates, the relative spatial profile shape is fairly constant along the axis, so a single point can stand for the whole amplitude quite well. Figure 6
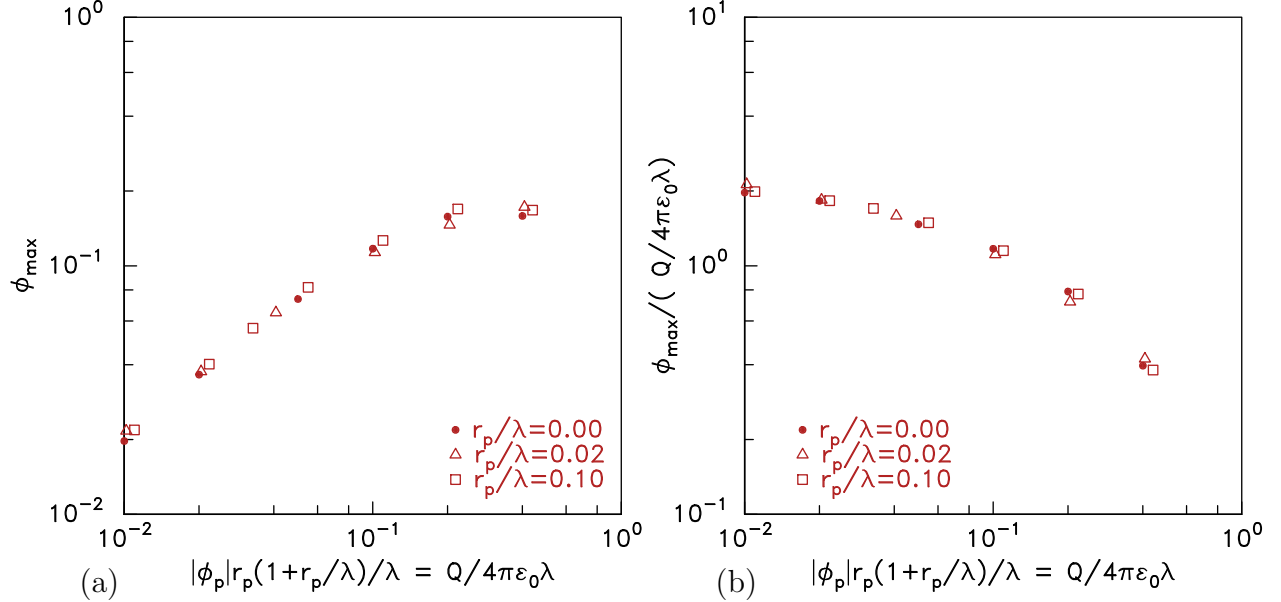

Figure 6: Variation of the wake maximum potential with object charge: (a) in units of T_e/e, and (b) normalized to particle charge. Parameters: $T_e/T_i = 100$, $M = 1$. Different object sizes are indicated with different symbols.

shows how the absolute and scaled ϕ_{max} varies with object charge. We see immediately that the size of the object is practically irrelevant. All three sizes give the same wake magnitude to within a few percent. This shows that absorption by the object is unimportant in these cases, even when r_p is fully ten percent of λ_{De}. Computations on a domain half the transverse size ($-25 < x, y < 25$) agree with these results within a few percent, establishing that the domain size used is big enough not to matter for ϕ_{max}. The absolute ϕ_{max} shows a saturation value just under $0.2(T_e/e)$ at large charges ($|\phi_p|r_P/\lambda_{De} \gtrsim 0.2$). But the nonlinear effects have begun to be important well before that, as Figure 6(b) most clearly shows. Linear response would correspond to scaled potential, ϕ_{max}/Q, independent of $|\phi_p|r_P/\lambda_{De}$. This independence is barely reached even for the smallest charges plotted, $|\phi_p|r_P/\lambda_{De} = 0.01$.

Naturally the shape of the wake depends upon the ion drift velocity (M). Figure 7 shows that the dominant variation is in the angle of the wavefronts in the wake. The angle between the wave-front-normal (effective k-direction) and the drift direction is reasonably approximated by $\tan\theta = M$. This is *not* the familiar simple form for a Mach cone, $\cos\theta = 1/M$. As has been observed by previous authors, the wake has this conical structure for both sub- and super-sonic drift velocities, which is of course not the case for a simple Mach-cone. The reason is presumably that the ion acoustic wave is strongly dispersive when $k\lambda_{De} \sim 1$, as invoked in [4].
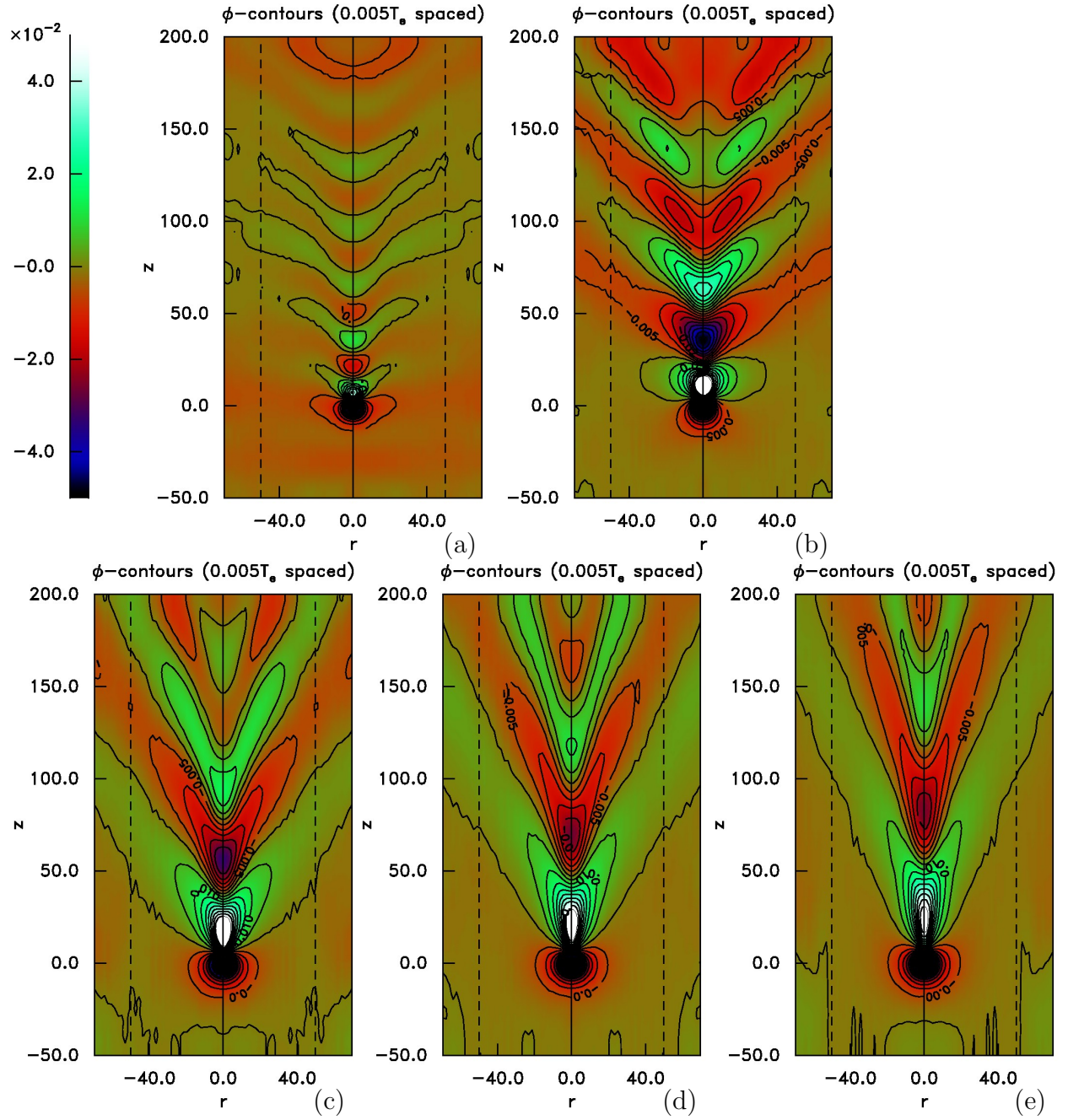
11

Figure 7: Wake structures for subsonic (a) $M = 0.5$, (b) $M = 0.8$, and supersonic (c) $M = 1.2$ (d) $M = 1.5$, (e) $M = 1.8$ cases. $T_e/T_i = 100$, $|\phi_p|r_p/\lambda_{De} = 0.05$, $\lambda_{De} = 10$, point-charge.
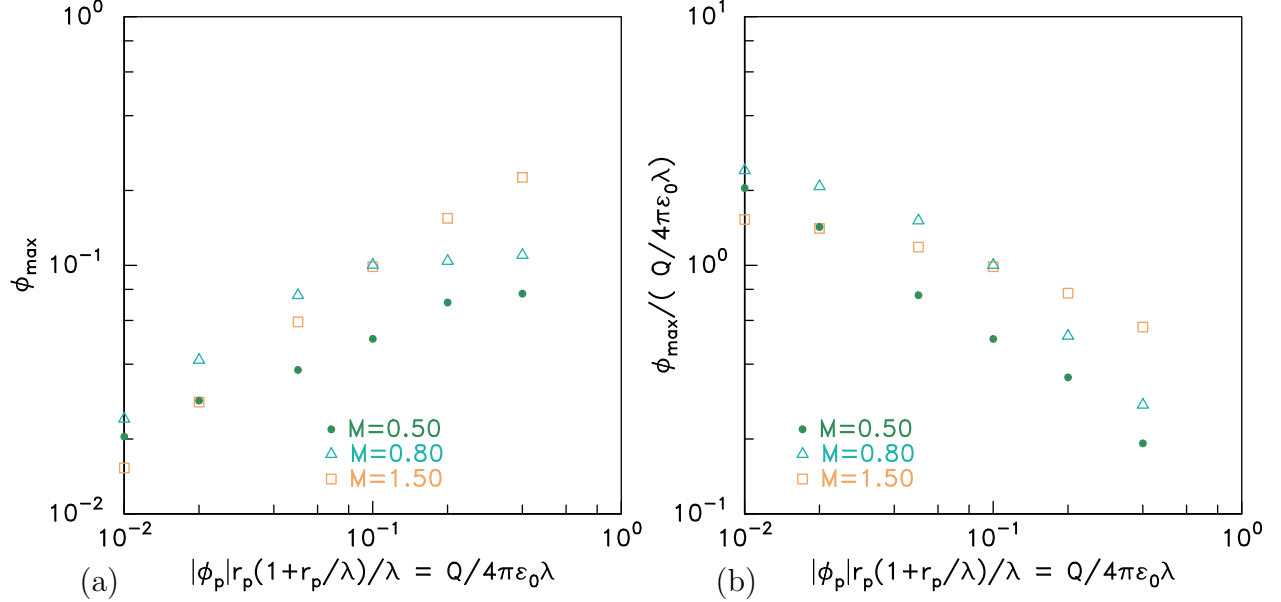
Figure 8: Variation of the wake maximum potential with drift velocity: (a) in units of T_e/e, and (b) normalized to particle charge. Parameters: $T_e/T_i = 100$, point-charge. Different drift Mach numbers (M) are indicated with different symbols.

At different drift velocities, saturation of the peak potential takes place somewhat differently, as shown in Fig. 8. Subsonic cases, $M = 0.5, 0.8$, are even further from being fully linear than was the case in Fig. 6, and are not in the linear regime at the lowest plotted normalized charge $|\phi_p| r_p/\lambda_{De} = 0.01$. The supersonic case is practically into the linear regime. At high charge, the subsonic cases show strong saturation of the peak potential, at levels decreasing, below $0.1 T_e/e$, with decreasing M. The supersonic case does not show saturation of the absolute peak potential, even above $0.2 T_e/e$. These trends are approximately consistent with a saturation mechanism that depends upon the ratio of peak potential energy to drift ion energy. Nonlinearity is significant when $e\phi_{max}/T_e M^2 \gtrsim 10^{-2}$, and saturation is essentially complete when $e\phi_{max}/T_e M^2 \gtrsim 0.2$. Although the data indicates this latter criterion is an over-simplification, it makes sense, since it amounts to a statement that the potential peak is high enough to reduce the particle kinetic energy by a factor of ~ 2. [An *a priori* argument based on the deviation of orbits at a marginal distance of λ_{De} would give a non-linearity criterion $(e\phi_p/T_e)(r_p/\lambda_{De}) \propto M^2$, which is also compatible with the above observations, but the constant of proportionality would be a guess without quantitative results like these.]

In Fig. 9 is shown the density (normalized to $n_{i\infty}$) for a substantially nonlinear case. The density enhancement caused by ion focusing immediately behind the particle is very large: a factor of 10 at the peak. This density peak is at a very short distance $z = 1.5 = 0.15\lambda_{De}$ downstream from the particle, much closer than the potential peak, which is at about $1.2\lambda_{De}$ (see Fig. 4). The density peak has an extremely narrow radius, with half-width only about $0.04\lambda_{De}$. Fortunately it does not prove necessary to resolve this peak very well when obtaining the potential, because of the smoothing effect of the Poisson equation. When the particle

13
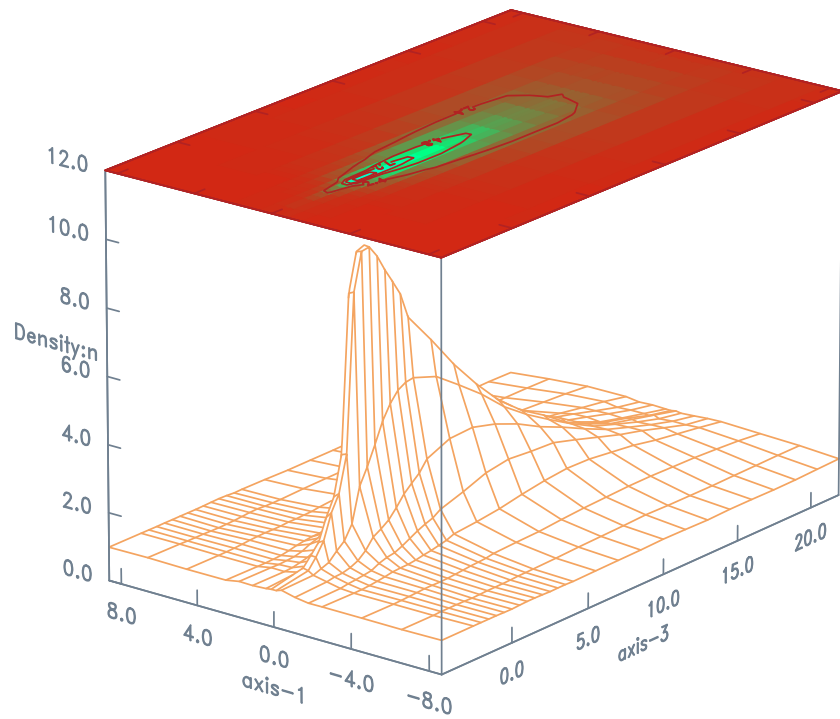
Dimension 2 Plane 16

Figure 9: Normalized density in the $y = 0$ plane close to a point-charge. Parameters: $T_e/T_i = 100$, $M = 1$, $|\phi_p|r_p/\lambda_{De} = 0.1$, $\lambda_{De} = 10$.

14

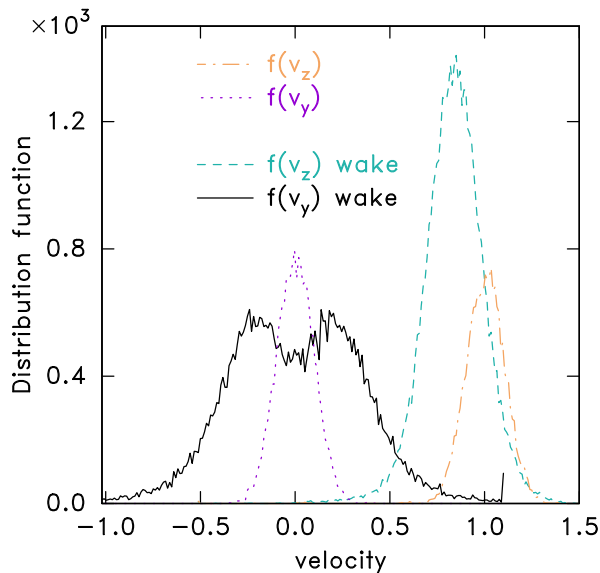charge is reduced, the linear regime is approached when the peak density is roughly 2.

Figure 10: Velocity distribution functions for the case of Fig. 9 in one velocity-dimension (y or z) integrated over the other dimensions. The cases marked "wake" are sampled over the density peak in a rectangular box $-2 < x, y < 2$, $1 < z < 15$. The others are unperturbed distributions sampled over an equal volume.

The ion velocity distribution shapes in the wake are strongly perturbed. Fig. 10 shows examples of the distribution averaged over the density peak, compared with distributions for an unperturbed region of the same case. The unperturbed distributions reflect the shifted Gaussian shape of the injected particles, with the z-velocity centered on the drift velocity $M = 1$. Velocities are normalized to $\sqrt{T_e/m_i}$. The ordinate is the number of particles in each of the equal velocity-interval boxes; so the statistical uncertainty is about equal to its square root. The wake distributions contain substantially more total particles because of the peaked local density. Their widths are greatly increased, for v_z mostly by deceleration, and for v_y by inward lateral acceleration which has produced a double-humped distribution. Wake effective ion temperatures far exceed the unperturbed $0.01 T_e$. So we expect much stronger Landau damping than the linearized (unperturbed) distribution would imply. As the charge value is lowered towards the linear regime (not shown), the distribution shape perturbation gradually disappears. Thus, a major effect of nonlinearity is local enhancement of the effective ion temperature and consequent damping.

4 Linear Comparisons

In comparing COPTIC results with prior linearized calculations we can draw some immediate qualitative conclusions. First, the longitudinal wavelength of oscillation is observed to be close to $2\pi\lambda_{De}M$, eq. (3), in agreement with the conclusions of [7, 8, 9, 11, 12, 10] but in

contradiction of [6] and more straightforwardly than implied by [4, 5]. Essentially all recent studies, including the present one, are in agreement that the wavelength is given by eq. (3) not eq. (2). The phase of the oscillations obtained in [9] is however clearly in disagreement with our results. In that work the first peak is over half a wavelength downstream of the charge, whereas COPTIC shows it to be no more than 0.2 times the wavelength downstream. In addition the decay of the oscillations we observe far exceeds that of [9, 10] for the same conditions (presumably because those approaches exclude Landau damping). Much the same discrepancies exist in comparison with [8]: its first peak is too far from the object and damping is much less. All of these differences exist in comparison with low amplitude almost linear COPTIC calculations, quite apart from issues of non-linearity. Since [7] gives only approximate forms, and [12] deals only with charge rods, the remaining possible quantitative comparison with theory appears to be with the work of Lampe et al in [11]. (The plots of [19] appear qualitatively consistent but include collisions, which are here omitted.)
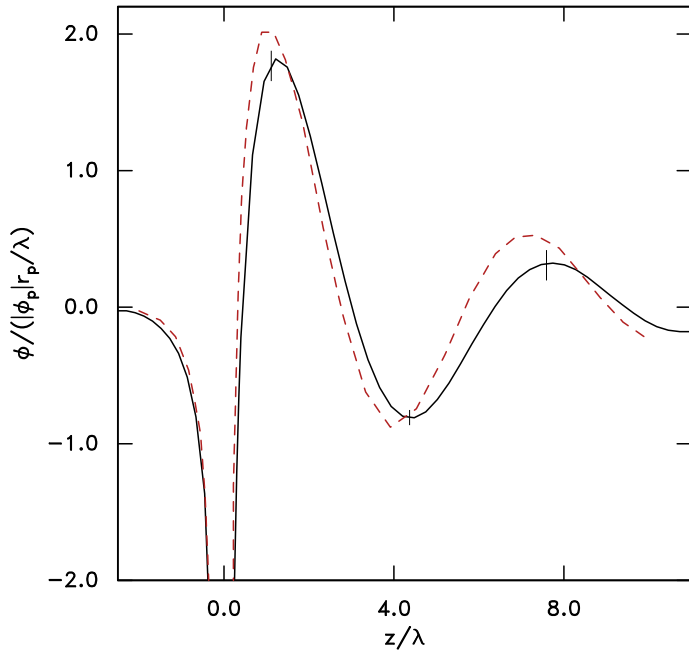

Figure 11: Comparison of potential along the $\hat{z}$-axis of flow. Solid curve is COPTIC's result for parameters $T_e/T_i = 50$, $M = 1$, for a point particle of charge $\phi_p r_p/\lambda_{De} = -0.005$. Dashed curve is the result of [11] figure 3, for the same parameters.

In Fig. 11 a comparison is shown between the potential along the axis for COPTIC and the result of figure 3 of [11]. Although it is not specified what the ϕ-scale of that figure is, the closeness of the values appears to confirm that it is normalized in the natural way chosen here. We observe that the agreement, while encouraging, is not perfect. The COPTIC wake peak amplitude is about 10% lower than the linear response calculation. This discrepancy might perhaps be attributable to insufficient spatial resolution in the COPTIC calculation, or low-level noise or non-linearity even at this charge level. The result shown is

16

from a computationally intensive run using about 280M particles to minimize the effective collisionality induced by noise. The error bars' half-height equals the uncertainty estimated by its deviation from a run based on 30M particles. The inconsistency in the wavelength, which is 10% shorter in Lampe et al's result than from COPTIC, cannot be explained on the basis of COPTIC uncertainty. The COPTIC wavelength is observed in other runs to be very insensitive to particle charge and mesh. The wavelength discrepancy's cause is therefore unknown. However, uncertainties in the linearized calculation (dashed line) are reported [25] to be probably 5% in amplitude and up to 10% in wavelength. So it appears that the discrepancies are within the uncertainty of both results.
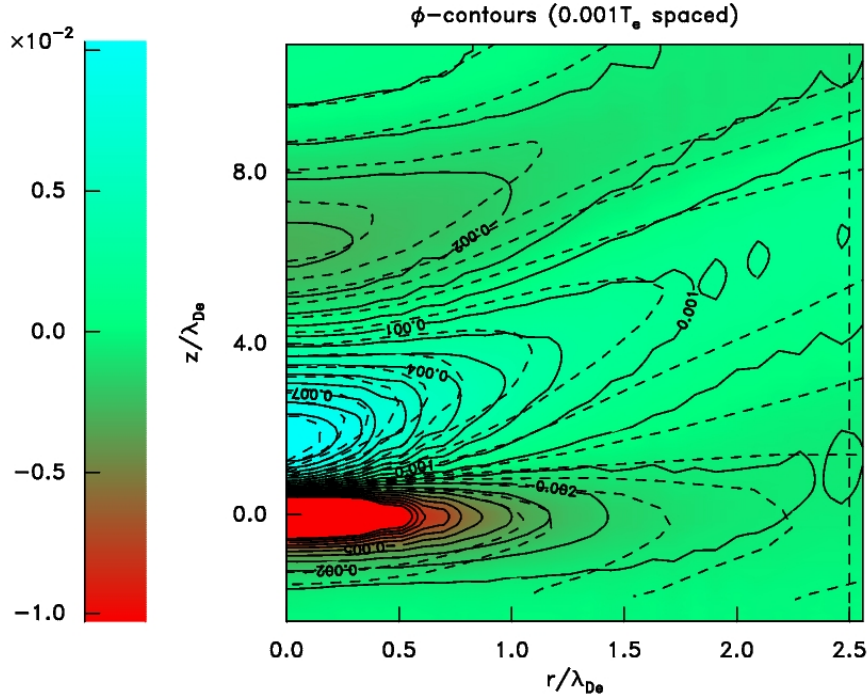

Figure 12: Contours of potential from COPTIC (solid curves) for $T_e/T_i = 25$, $M = 1.5$, $\phi_p r_p/\lambda_{De} = 0.01$, point-charge, and from ref [11] figure 2 (dashed curves).

Fig. 12 is a comparison of potential contours in radius and longitudinal position. The contour values of figure 2 of [11] are not specified, but appear to coincide with the spacing chosen here. In any case, it is the shape that is most significant. Once again the qualitative features are generally in excellent agreement, but there are small quantitative discrepancies. The total number of contours along the z-axis between the peak (at about $2.5\lambda_{De}$ and the first subsidiary valley (at about 6.5) are the same. But the dashed contours *trail* the solid COPTIC contours behind the first potential peak (around 5.0) by over one contour. In other words, the dashed contours in that region are at larger z than their corresponding solid contours. This is the *opposite* sign of discrepancy to that observed in Fig. 11, in which the linear-response result leads. The other significant discrepancy is that the linear-response contours at the leading edge (bottom) of the box extend further to the upstream than those

of COPTIC. It is hard to know how much significance to place on these minor discrepancies.

5 Consistency with Experiments

Examination of the cone-like form of the potential suggests an explanation of the experimental observations of Hebner and Riley: that dissimilar particles, which naturally float in a sheath at different heights, sometimes align obliquely at small angles (from 30 degrees downwards) to the vertical. First we note that, if we suppose that only the electric potential (not e.g. ion drag force) is important, the natural interparticle distance for two particles vertically aligned is equal to the distance of the first downstream potential peak. In the present simulations, this is approximately $1.2M\lambda_{De}$. In [21] the observed distance for vertically aligned particles was observed to be approximately $1.5\lambda_{De}$, which is not unreasonable. However, one must take into account the external potential well that arises from the balance of vertical forces. In the limit in which this potential well is *stronger* than the wake fields, so that the height is controlled by the external sheath dynamics, we can readily deduce the horizontal equilibrium position. Incidentally this limit seems likely most often to be appropriate, since as has been shown here, the wake potential is severely limited by non-linearities. In [22] the attractive potential wake peak was estimated to be no larger than 21mV in a $T_e \sim 3$eV plasma (consistent with being near the upper limit of the linear regime). If the external sheath structure dominates, the particles are constrained to be at some fixed vertical distance apart dependent upon their different sizes. The downstream particle is therefore attracted to the peak of the wake potential *at a fixed z-position*. The transverse position of this maximum can readily be deduced from the wake potential contours plotted in prior figures. When the z-position is such as to intersect the axial wake peak, the particle will align on axis (angle equals zero). However if the z-displacement is such as to intersect the positive-potential cone *off-axis*, then it will align off-axis, at the peak of the cone potential. Examination of Fig. 5(b) shows that the potential peaks off-axis only for $z \gtrsim 25 = 2.5\lambda_{De}$ when $M = 1$, while from Fig. 7(b) (or Fig. 12 at higher T_i) when $M = 1.5$ the condition is $z \gtrsim 3.7\lambda_{De} \approx 2.5M\lambda_{De}$. At $M = 1.5$, the cone persists at least to $z = 8\lambda_{De}$. Mach numbers below 1, e.g. Fig. 7(a), have flatter cone-angle and less-pronounced cone-structures but might perhaps be able to sustain off-axis alignment. The experiments of [22] observed off-axis alignment only for the larger vertical displacements $\gtrsim 3.5\lambda_{De}$ (although the value of λ_{De} itself is subject to considerable uncertainties). This observation favors an effective M somewhat greater than 1. The angle of the peak potential alignment to the upstream particle is relatively small. The effects of collisions on the wake and the effect of ion drag on the forces are of course omitted from this estimate. Moreover the present calculations do not account for the varying external plasma sheath structure. Nevertheless, this comparison is encouraging. It appears that the small-angle offset from vertical alignment observed in some experiments for unlike particles is consistent with the downstream particle being attracted to the off-axis peak of the wake potential when the flow velocity is mildly supersonic.

6 Conclusion

The behavior of the wake of a sphere in a flowing plasma has been calculated fully non-linearly. Quantitative comparisons with linear response calculations using the full kinetic dielectric response are reasonably satisfactory for small enough charge. But the present work shows that non-linearity affecting the entire wake begins at quite low charge level, corresponding to a floating sphere radius about 10^{-2} of the Debye length. Examples of the potential, density, and ion velocity distribution show the large perturbations and wide range of scales that are involved in this complex problem.

7 Acknowledgements

References

[1] N. Rostoker, Nucl. Fusion **1**, 101 (1961).

[2] J. H. Chu and I. Lin, Phys. Rev. Lett. **72**, 4009 (1994).

[3] A. Melzer, V. Schweigert, I. Schweigert, A. Homann, S. Peters, and A. Piel, Phys. Rev. E **54**, R46 (1996).

[4] J. Sanmartin and S. Lam, Phys. Fluids **14**, 62 (1971).

[5] L. Chen, A. Langdon, and M. Lieberman, J. Plasma Phys. **9**, 311 (1973).

[6] O. Ishihara and S. V. Vladimirov, Phys. Plasmas **4**, 69 (1997).

[7] B. Xie, K. He, and Z. Huang, Phys. Lett. A **253**, 83 (1999).

[8] D. S. Lemons, M. S. Murillo, W. Daughton, and D. Winske, Phys. Plasmas **7**, 2306 (2000).

[9] G. Lapenta, Phys. Rev. E **63**, 1175 (2000).

[10] L.-J. Hou, Y.-N. Wang, and Z. L. Miskovic, Phys. Rev. E. **64**, 046406 (2001).

[11] M. Lampe, G. Joyce, G. Ganguli, and V. Gavrishchaka, Phys. Plasmas **7**, 3851 (2000).

[12] D. Winske, W. Daughton, D. Lemons, and M. Murillo, Phys. Plasmas **7**, 2320 (2000).

[13] W. J. Miloch, J. Trulsen, and H. L. Pecseli, Phys. Rev. E **77**, 056408 (2008).

[14] I. H. Hutchinson, in *New Vistas in Dusty Plasmas*, edited by L. Bounfendi and M. Mikikian (AIP, 2005) pp. 38–47, Proc. 4th Int. Conf. on Physics of Dusty Plasmas, Orléans.

[15] K. Takahashi, T. Oishi, K.-i. Shimomai, Y. Hayashi, and S. Nishino, Phys. Rev. E **58**, 7805 (1998).

[16] A. Melzer, V. Schweigert, and A. Piel, Phys. Rev. Lett. **83**, 3194 (1999).

[17] V. Steinberg, R. Sütterlin, A. V. Ivlev, and G. Morfill, Phys. Rev. Lett. **86**, 4540 (2001).

[18] A. A. Samarian, S. V. Vladimirov, and B. W. James, Phys. Plasmas **12**, 022103 (2005).

[19] M. Lampe, G. Joyce, and G. Ganguli, IEEE Trans. Plasma Sci. **33**, 57 (2005).

[20] M. Kroll, J. Schablinski, D. Block, and A. Piel, Phys. Plasmas **17**, 013702 (2010).

[21] G. Hebner and M. Riley, Phys. Rev. E **68**, 046401 (2003).

[22] G. Hebner and M. Riley, Phys. Rev. E **69**, 026405 (2004).

[23] N. Matsunaga and T. Yamamoto, J. Comp. Appl. Math. **116**, 263 (2000).

[24] R. W. Hockney and J. W. Eastwood, *Computer Simulation using Particles* (Taylor and Francis, London, 1988).

[25] M. Lampe(2010), private communication.